A new role for the architecture of microvillar actin bundles in apical retention of membrane proteins

Céline Revenu[a,*,†], Florent Ubelmann[a,*], Ilse Hurbain[a,b], Fatima El-Marjou[a], Florent Dingli[c], Damarys Loew[c], Delphine Delacour[d], Jules Gilet[e], Edith Brot-Laroche[e], Francisco Rivero[f], Daniel Louvard[a], and Sylvie Robine[a]

[a]Unité Mixte de Recherche 144, Centre National de la Recherche Scientifique, [b]Cell and Tissue Imaging Facility-IbiSA, and [c]Laboratory of Proteomic Mass Spectrometry, Institut Curie, 75248 Paris, Cedex 05, France; [d]Institut Jacques-Monod, CNRS-UMR7592, Paris 7 University, 75013 Paris, France; [e]Centre de Recherche des Cordeliers, Université Pierre et Marie Curie, UMR S 872, 75006 Paris, France; [f]Centre for Cardiovascular and Metabolic Research, The Hull York Medical School, and Department of Biological Sciences, University of Hull, Hull HU6 7RX, United Kingdom

ABSTRACT **Actin-bundling proteins are identified as key players in the morphogenesis of thin membrane protrusions. Until now, functional redundancy among the actin-bundling proteins villin, espin, and plastin-1 has prevented definitive conclusions regarding their role in intestinal microvilli. We report that triple knockout mice lacking these microvillar actin-bundling proteins suffer from growth delay but surprisingly still develop microvilli. However, the microvillar actin filaments are sparse and lack the characteristic organization of bundles. This correlates with a highly inefficient apical retention of enzymes and transporters that accumulate in subapical endocytic compartments. Myosin-1a, a motor involved in the anchorage of membrane proteins in microvilli, is also mislocalized. These findings illustrate, in vivo, a precise role for local actin filament architecture in the stabilization of apical cargoes into microvilli. Hence, the function of actin-bundling proteins is not to enable microvillar protrusion, as has been assumed, but to confer the appropriate actin organization for the apical retention of proteins essential for normal intestinal physiology.**

Monitoring Editor
Keith E. Mostov
University of California, San Francisco

Received: Sep 7, 2011
Revised: Oct 19, 2011
Accepted: Nov 16, 2011

This article was published online ahead of print in MBoC in Press (http://www.molbiolcell.org/cgi/doi/10.1091/mbc.E11-09-0765) on November 23, 2011.

*These authors contributed equally to this work.

†Present address: EMBL, 69126 Heidelberg, Germany.

Address correspondence to: Céline Revenu (revenu@embl.de) or Sylvie Robine (sylvie.robine@curie.fr).

Abbreviations used: APN, aminopeptidase N; DAPI, 4′,6-diamidino-2-phenylindole; DPPIV, dipeptidylpeptidase IV; DTT, dithiothreitol; EGTA, ethylene glycol tetraacetic acid; $EP^{-/-}$, espin/plastin-1 double KO mice; FCS, fetal calf serum; IAP, intestinal alkaline phosphatase; KO, knockout; LPH, lactase phlorizin hydrolase; OCT, optimal cutting temperature compound; $P^{-/-}$, plastin-1 KO mice; PBS, phosphate-buffered saline; PepT1, peptide transporter protein T1; PFA, paraformaldehyde; SI, sucrase-isomaltase; TEM, transmission electron microscopy; $VE^{-/-}$, villin/espin double KO mice; $VEP^{-/-}$, villin/espin/plastin-1 triple KO mice; $VP^{-/-}$, villin/plastin-1 double KO mice; WT, wild type.

INTRODUCTION

Epithelia constitute the interface between an organ or organism and its environment. This interface ensures a selective barrier that enables protection from external aggressions while allowing necessary exchanges with the surroundings. Most epithelia are indeed specialized in the secretion and/or absorption of various molecules. This functional interface requires a tight sealing of epithelial cells with their neighbors and an asymmetrical subcellular organization between the external (apical) and internal (basal) domains of the epithelial cell. The mechanisms responsible for this striking structural and functional separation between the apical and basal domains are beginning to be well understood. It is clear that complex sorting and cargo-trafficking machineries are essential for the establishment of epithelial cell polarity (Rodriguez-Boulan *et al*., 2005; Sato *et al*., 2007; Weisz and Rodriguez-Boulan, 2009).

The absorptive cells of the intestine, termed enterocytes, represent the archetype of apico-basal polarity in epithelial cells. Tight and adherens junctions separate a basolateral domain from the

brush border, a highly differentiated apical pole structure composed of a dense array of finger-like protrusions: the microvilli. The brush border considerably increases apical cell surface area for the exposure of membrane-bound hydrolases, which participate in the last step of extracellular digestion, and channels and transporters for nutrient uptake. Intestinal microvilli are supported by parallel arrays of actin filaments that create a paracrystalline arrangement: the actin bundle. Actin filaments are constantly polymerizing at the tip of each bundle, but the mechanism of nucleation of the actin network is still unknown. The actin network is linked to the plasma membrane via myosin-1a bridges (Coluccio and Bretscher, 1989), whereas its rootlets expand into the cytoplasm and are connected to the actin and intermediate filaments of the terminal web (Hirokawa *et al.*, 1982, 1983). The ERM protein ezrin participates in the organization of this terminal web region and in the proper shaping of microvilli (Saotome *et al.*, 2004). A capping and cross-linking protein present at the plus end of the filaments, Eps8, has also been implicated in the regulation of microvillar morphogenesis (Croce *et al.*, 2004). Three actin-bundling proteins, villin, plastin-1, and espin, are present in intestinal microvilli. Actin-bundling proteins represent a subset of actin cross-linking proteins, as they are able not only to bind several filaments to create an undefined network, but also to organize filaments in a regular, tight, parallel array to form a bundle; the latter can only be demonstrated by electron microscopy. We will therefore refer in this paper to actin-bundling proteins using this strict definition of proteins that build a paracrystalline bundle.

Stereocilia, bristles, and filopodia are, as microvilli, membrane protrusions supported by parallel bundles of actin filaments (reviewed in Revenu *et al.*, 2004). These actin-based structures all contain several actin-bundling proteins thought to be essential for the formation of the protrusions (Bartles, 2000). Indeed, the down-regulation of the bundler fascin induces a decrease of filopodia number and the remaining ones are short and bent, running nearly parallel to the membrane (Vignjevic *et al.*, 2006). Conversely, fascin overexpression and constitutive activation produce numerous filopodia (Yamashiro *et al.*, 1998; Vignjevic *et al.*, 2006). In *Drosophila melanogaster*, forked or fascin mutants strongly affect bristle morphogenesis (Tilney *et al.*, 1995, 1998). In the jerker mouse, the absence of espin destabilizes inner ear stereocilia, leading to their degeneration (Zheng *et al.*, 2000). Finally, in cells in culture, the ectopic expression of villin in a fibroblastic cell line induces the formation of microvillus-like protrusions (Friederich *et al.*, 1989; Franck *et al.*, 1990), whereas its down-regulation disrupts brush border maintenance in a polarized colonic cell line (Costa de Beauregard *et al.*, 1995). In light of these results, it was proposed that bundling proteins confer requisite stiffness for the actin network to deform the membrane and extend a straight protrusive structure.

However, knockout (KO) of the gene encoding villin in mice did not lead to any detectable morphological defect in the enterocyte brush border (Pinson *et al.*, 1998; Ferrary *et al.*, 1999). Similarly, we were unable to observe an alteration of the organization of intestinal microvilli in jerker mice lacking espins (unpublished data). The loss of plastin-1 predominantly affects the organization of the terminal web, although a slight reduction in the length of microvilli was reported (Grimm-Gunter *et al.*, 2009). Thus none of the three actin-bundling proteins is individually essential for the formation and maintenance of intestinal microvilli. Redundancy among the three actin-bundling proteins was proposed to account for the robustness of the system and therefore for the lack of phenotypes in all the single KO studied.

In the present study, we investigate the function of actin-bundling proteins in intestinal microvilli by circumventing these possible compensatory mechanisms through the analysis of double and triple KO of the three actin-bundling proteins of the intestinal brush border in mice. We demonstrate that the bundled architecture of actin filaments is not primarily necessary for microvilli morphogenesis but is essential for the proper recruitment of key players in the apical membrane anchorage of digestive and absorptive proteins.

RESULTS

Villin/espin/plastin-1 triple KO mice show growth defects

To investigate redundancy among the three actin-bundling proteins of enterocytic microvilli—villin, plastin-1 and espin—we crossed the corresponding single KO (Ferrary *et al.*, 1999; Zheng *et al.*, 2000; Grimm-Gunter *et al.*, 2009) to obtain all four possible combinations: villin/espin, villin/plastin-1, and espin/plastin-1 double KO mice ($VE^{-/-}$, $VP^{-/-}$, and $EP^{-/-}$ mice, respectively) and villin/espin/plastin-1 ($VEP^{-/-}$) triple KO mice. All these mice are viable and fertile. The double KO animals appear normal with the exception of mice lacking espin, which have behavioral defects, as described previously (Gruneberg *et al.*, 1941). The $VEP^{-/-}$ mice demonstrated a smaller body size compared with wild-type (WT) animals (Figure 1A). $VEP^{-/-}$ mice consistently showed a statistically significant growth delay during their first 60 d of life for both males and females compared with their triple heterozygote ($VEP^{+/-}$) half-sibling and double KO $VP^{-/-}$ controls. No significant difference in the growth of $VEP^{+/-}$ and $VP^{-/-}$ mice was found (Figure 1B). The growth delay of $VEP^{-/-}$ mice became more pronounced at ~20–25 d, which corresponds to the weaning period (Figure 1B). Thus $VEP^{-/-}$ mice suffer from growth retardation for the duration of their first 60 d of growth.

The global organization of the enterocytes of $VEP^{-/-}$ mice is preserved

Despite displaying a growth retardation phenotype, the global crypt–villus organization of the intestinal epithelium of $VEP^{-/-}$ mice does not show any overt defects, as was revealed by hematoxilin-eosin staining (Figure 1C). Intestinal sections from $VEP^{-/-}$ mice demonstrated normal apical concentrations of ezrin and F-actin compared with WT sections (Figure 1C). The lateral and apical-lateral junctional markers E-cadherin and ZO-1 also retained their expected localizations in the $VEP^{-/-}$ enterocytes. Therefore, even in the absence of all three actin-bundling proteins, the intestinal epithelial organization and polarity appeared normal at the tissue level. We then investigated the distribution of the main cytoskeletal elements at the cellular level (Figure 1D). In the $VEP^{-/-}$ enterocytes, microtubules showed the classical, mainly apico-basal orientation, and keratin filaments presented a normal diffuse pattern with a slight concentration in the terminal web as in enterocytes from WT mice. At this cellular resolution, the strong brush border localization of actin filaments, although maintained, often appeared narrower in the $VEP^{-/-}$ compared with the WT mice, suggesting an alteration at the level of the microvilli (Figure 1D). Therefore the growth delay present in $VEP^{-/-}$ mice does not seem to be caused by abnormalities in intestinal morphology or global polarity of enterocytes.

Intestinal microvilli form even in the absence of the three actin-bundling proteins

Given the proposed role of actin-bundling proteins in the formation of membrane protrusions, we used transmission electron microscopy (TEM) to investigate the defects generated by the combined absence of two or three bundling proteins in intestinal microvilli morphogenesis. Unexpectedly, microvilli were present in all KO mice analyzed, even in the absence of the three bundlers (Figure 2, A and B). Although TEM confirmed the global preservation of the

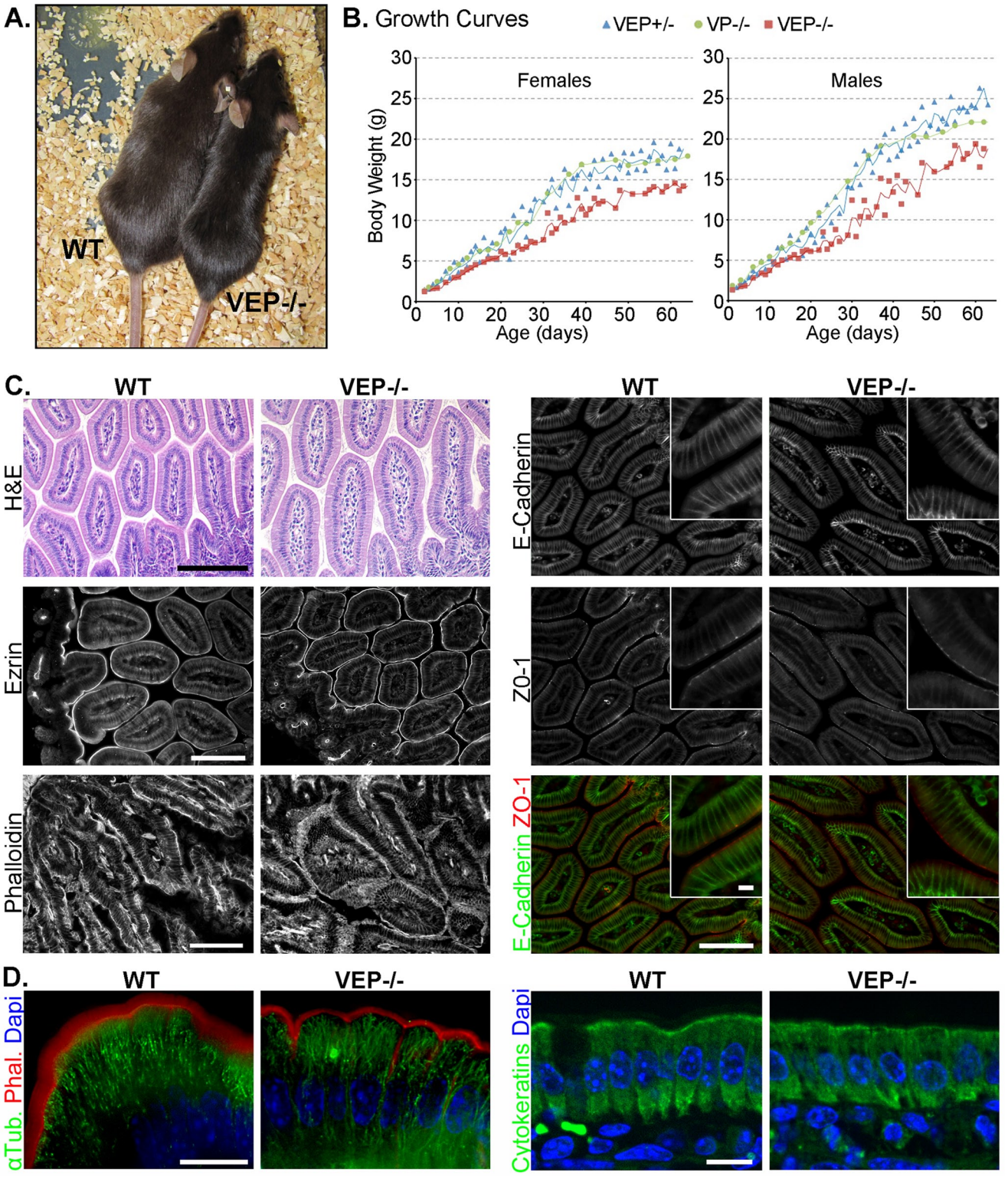

FIGURE 1: The VEP$^{-/-}$ mice have growth defects, but the morphology of their intestinal epithelium looks normal. (A) Picture of a triple KO VEP$^{-/-}$ animal next to a WT animal of the same age. (B) Growth curves plotting the average weight of 35 triple heterozygotes (VEP$^{+/-}$), 16 villin/plastin-1 double KO (VP$^{-/-}$), and 35 triple KO (VEP$^{-/-}$) mice according to their age. Males and females were analyzed separately. (C and D) Histological sections of jejunum from WT and triple KO (VEP$^{-/-}$) animals. (C) H&E shows a hematoxilin and eosin staining (scale bar: 200 μm), phalloidin labels F-actin (scale bar: 100 μm). Immunostaining for ezrin, E-cadherin, and ZO-1 is shown. Scale bars: 100 μm; insets: 10 μm. (D) The global cellular organization of the cytoskeletal elements is presented. Microtubules and F-actin are revealed by immunostaining against α-tubulin (α-Tub., green) and phalloidin labeling (Phal., red). Cytokeratins are labeled with a pancytokeratin antibody (green); 4′,6-diamidino-2-phenylindole (DAPI) labels nuclei (blue). Scale bars: 10 μm.

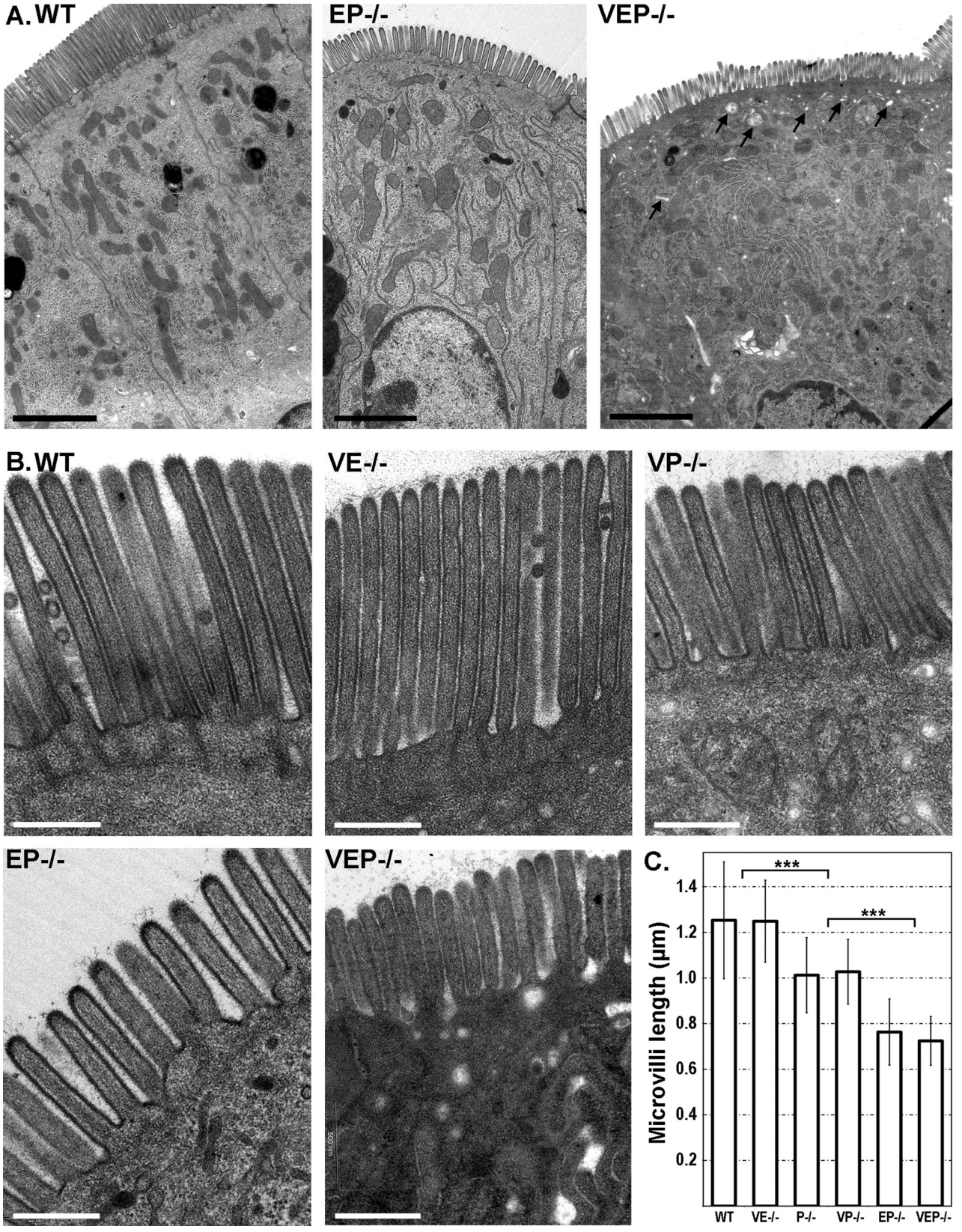

FIGURE 2: Microvilli still form in the VEP$^{-/-}$ mice. (A) Transmission electron micrographs of sections of jejunum from WT, EP$^{-/-}$, and VEP$^{-/-}$ presenting a general view of the enterocyte polarity. Arrows point at apical vesicles and vacuoles in the VEP$^{-/-}$ sample. Scale bars: 2 µm. (B) Transmission electron micrographs of sections of jejunum from WT, the three double KO (VE$^{-/-}$, VP$^{-/-}$, EP$^{-/-}$) and the triple KO (VEP$^{-/-}$) mice illustrating the organization of the brush border. Scale bars: 500 nm. (C) Histograms illustrating the average lengths of the intestinal microvilli depending on the genotype. Values are 1.25 ± 0.26 µm, n_{WT} = 86; 1.01 ± 0.16 µm, $n_{P-/-}$ = 194; 1.03 ± 0.14 µm, $n_{VP-/-}$ = 14; 0.76 ± 0.15 µm, $n_{EP-/-}$ = 75; 0.72 ± 0.11 µm, $n_{VEP-/-}$ = 58. *** *t* test $p < 0.001$.

apico-basal polarity of the enterocytes, with a well-defined brush border facing the lumen, the cytoplasm of the VEP$^{-/-}$ cells demonstrated a higher concentration of vesicles, vacuoles, and tubular structures, especially in the apical area, compared with WT enterocytes. This was quantified by evaluating the number of vesicular structures per square micrometer in the first apical micron of cytoplasm below the microvilli (1.74 ± 0.94, n_{WT} = 5 cells; 7.63 ± 0.52, $n_{VEP-/-}$ = 6 cells; Mann-Whitney $p < 0.01$; Figure 2A). We could not detect any defect in the brush border of the VE$^{-/-}$ mice. The VP$^{-/-}$, EP$^{-/-}$, and VEP$^{-/-}$ mice showed defects similar to those reported for the plastin-1 KO mice (P$^{-/-}$; Grimm-Gunter *et al.*, 2009), namely, very short or absent actin bundle rootlets and a strong reduction in the apical organelle free zone (Figure 2B).

Although the bundlers appeared nonessential for the formation of microvilli per se, they did have an effect on microvillar length (Figure 2C). Compared with microvilli of WT animals, the microvilli of VP$^{-/-}$ mice presented a reduction in length of ~20%, similar to the P$^{-/-}$ mice (1.03 ± 0.14 µm, $n_{VP-/-}$ = 14, and 1.01 ± 0.16 µm, $n_{P-/-}$ = 194, compared with 1.25 ± 0.26 µm, n_{WT} = 86; *t* test $p < 0.0001$). The EP$^{-/-}$ and the VEP$^{-/-}$ mice showed a major decrease in length of around 40% of the length of WT microvilli (0.76 ± 0.15 µm, $n_{EP-/-}$ = 75, compared with WT, *t* test $p < 0.0001$; 0.72 ± 0.11 µm, $n_{VEP-/-}$ = 58, compared with WT, *t* test $p < 0.0001$). The VEP$^{-/-}$ and EP$^{-/-}$ microvilli were thus very similar, with an average length of 724 and 763 nm, respectively, against 1253 nm for WT microvilli. Nevertheless, VEP$^{-/-}$ microvilli appeared less homogeneous in length per cell and less straight compared with EP$^{-/-}$ and a fortiori to WT microvilli (Figure 2, A and B). This was confirmed by the significantly increased coefficient of variation of the length of microvilli per cell in the VEP$^{-/-}$ compared with WT cells (2.54 ± 1.37%, n_{WT} = 7 cells, and 10.85 ± 4.90%, $n_{VEP-/-}$ = 7 cells; Mann-Whitney $p < 0.01$). In conclusion, the absence of the three known actin-bundling proteins reduces microvillar length but does not prevent microvillar protrusion. Providing that no additional actin-bundling protein compensates for the triple KO, it would appear that actin-bundling proteins are not required for membrane protrusion.

The loss of the three bundlers appears not to be compensated

To look for a fourth, unknown actin-bundling protein or for a protein compensating for the absence of the three bundlers that would account for the protrusion of microvilli in the VEP$^{-/-}$ enterocytes, we performed mass spectrometric analysis of the total protein content of WT and VEP$^{-/-}$ isolated brush borders. The list of actin-related proteins found in the analysis of WT brush borders is presented in Supplemental Table S1. All the additional proteins found in the analysis of VEP$^{-/-}$ brush borders are listed in Table S2, and the proteins missing in the VEP$^{-/-}$ compared with the WT brush borders are in Table S3. The potential cross-linkers harmonin and Eps8 could be detected in WT and VEP$^{-/-}$ brush borders. However, only the short harmonin isoform, harmonin a, which lacks the actin-bundling region (Verpy *et al.*, 2000), but not the cross-linking isoform b (Boeda *et al.*, 2002), could be detected in WT and VEP$^{-/-}$ brush borders by Western blot analysis using a pan-harmonin antibody (Supplemental Figure S1B). The capping protein Eps8 has also been recently proposed to have cross-linking activity in vitro that is enhanced by binding to IRSp53 (Disanza *et al.*, 2006; Hertzog *et al.*, 2010). IRSp53 was absent from both WT and VEP$^{-/-}$ brush borders, as we could neither find it in the proteomic data nor detect it by Western blotting (Figure S1A). Moreover, Eps8 expression levels were unchanged between WT and VEP$^{-/-}$ brush borders and, importantly, Eps8 was strictly localized at the very tip, as expected, and did not extend along the shaft of the microvilli in the VEP$^{-/-}$ samples (Figure S1A). Eps8 is thus not ectopically recruited and does not compensate for the loss of the actin-bundling proteins in VEP$^{-/-}$ intestinal microvilli. Finally, two interesting nucleators of linear actin filaments were detected in this proteomic study: cordon-bleu and diaphanous homologue 1. Cordon-bleu localized to the terminal web region and not to the tips of microvilli, as demonstrated by immunofluorescence (Figure S1C), and is thus unlikely to have a role in microvilli protrusion. The presence of diaphanous homologue 1 was confirmed by Western blotting (Figure S1C), but the lack of antibodies suitable for immunofluorescence prevented us from addressing its localization. No extra actin-bundling or cross-linking proteins could be detected in the VEP$^{-/-}$ brush borders compared with WT (Table S2). Thus the formation of microvilli in VEP$^{-/-}$ mice does not appear to be due to the compensatory recruitment of a fourth bundler but is more likely explained by the presence of the remaining actin-binding proteins normally present in microvilli.

The organization of F-actin into a bundle is lost in VEP$^{-/-}$ microvilli

We next addressed the precise organization of actin filaments, which were detected in microvilli after phalloidin staining (Figure 1D). The longitudinal striation due to the actin bundle was easily detectable by TEM in the double KO microvilli, whereas it was no longer distinguishable in the VEP$^{-/-}$ microvilli (Figure 2B). TEM of transverse sections of WT microvilli demonstrated a sharp, electron-dense, dotted pattern that corresponded to transverse sections of individual actin filaments (Figure 3A, insets). This pattern was absent in VEP$^{-/-}$ samples, which displayed only a few, indistinct darker areas that likely correspond to actin filaments (Figure 3A). This prevented the quantification of the number of filaments in VEP$^{-/-}$ samples. Noticeably, although the reticular organization of microvilli was unaffected as measured by the angle between three adjacent microvilli (65.9 ± 9.7°, n_{WT} = 115; 62.4 ± 9.4°, $n_{VEP-/-}$ = 151), the transverse area of microvilli was strongly decreased in VEP$^{-/-}$ versus WT animals (5231.1 ± 836.7 nm^2, $n_{VEP-/-}$ = 91, and 8909.5 ± 1097.9 nm^2, n_{WT} = 137; *t* test $p < 0.0001$; Figure 3B). As the number of filaments in the bundle influences the diameter of a protrusion (Tilney and Tilney, 1988), this could indicate a reduced number of filaments in the VEP$^{-/-}$ microvilli. In support of this hypothesis, Western blotting revealed that the actin content of the purified brush borders was reduced in VEP$^{-/-}$ mice compared with WT controls, whereas the actin content of enterocytes remained unmodified between WT and VEP$^{-/-}$ total lysates (Figure 3C).

To achieve better resolution of the actin filaments in microvilli, we performed TEM on isolated brush borders from WT and VEP$^{-/-}$ mice. This technique eliminates most of the background generated by the cytoplasmic elements, while the brush border actin cytoskeleton and its associated plasma membrane are preserved. As demonstrated by phalloidin staining, VEP$^{-/-}$ brush borders appeared thinner than WT brush borders and retained F-actin (Figure 3, D and E, insets). TEM revealed that longitudinal actin filaments were still present in VEP$^{-/-}$ microvilli. However, they lost the normal bundled structure present in the WT situation (compare Figure 3E with 3D): the number of filaments seemed to be reduced, and their spacing was highly irregular. In some areas, actin filaments appeared compacted and indistinguishable from each other, or even interrupted, which could be due to wavy filaments going out of the section. In other areas, the spacing between two filaments was enlarged compared with the WT bundle. This disorganization explains the lack of sharp actin dots in the transverse sections (Figure 3A). On the contrary, actin filaments in WT microvilli showed the expected highly

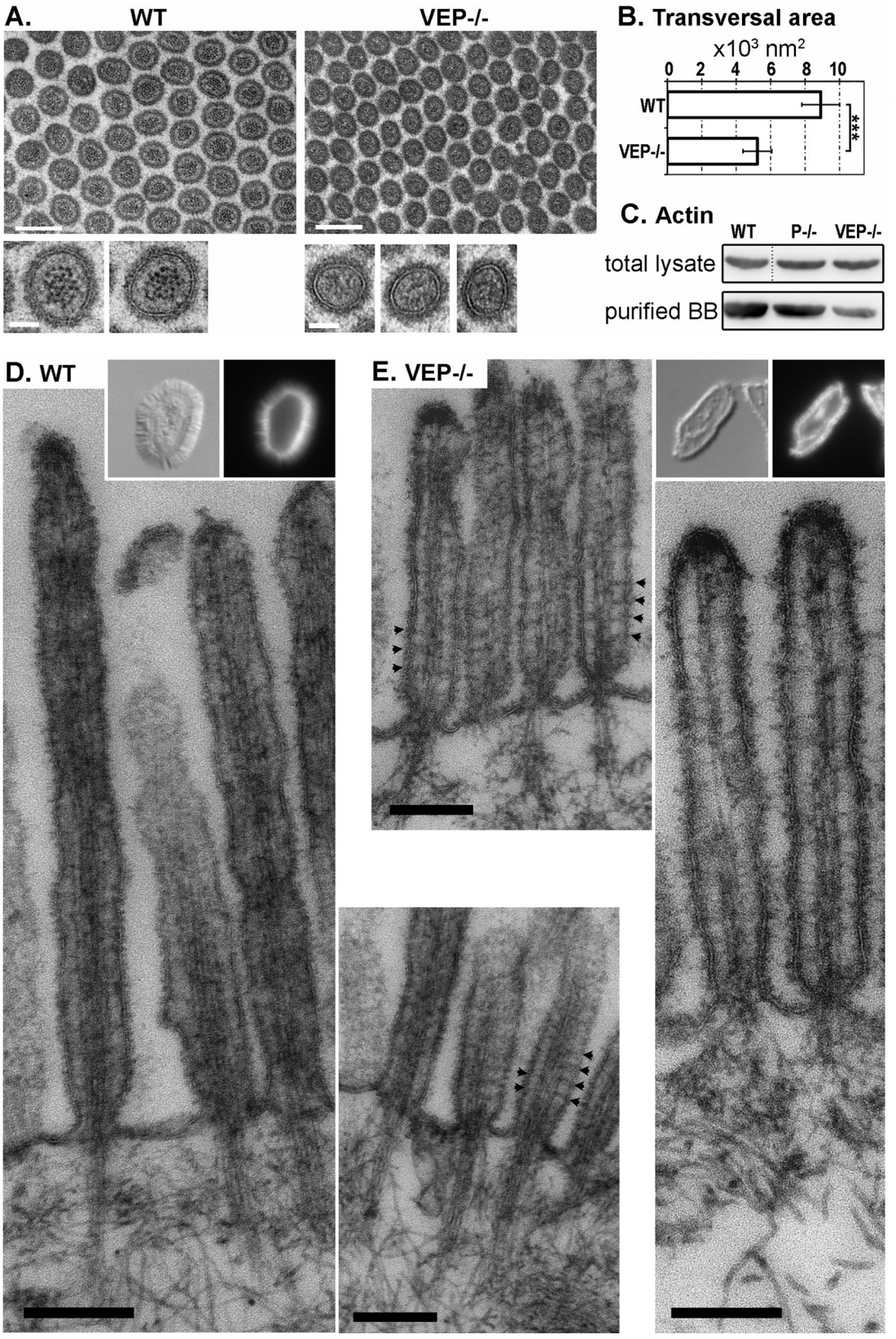

FIGURE 3: The organization of the actin bundle is affected in the VEP$^{-/-}$ microvilli. (A) Transmission electron micrographs of transversal sections of the microvilli of WT and VEP$^{-/-}$ mice. Scale bars: 200 nm; insets: 50 nm. (B) Histograms depicting the average area of transversal sections of microvilli depending on the genotype: 5231.1 ± 836.7 nm^2, $n_{VEP-/-}$ = 91 and 8909.5 ± 1097.9 nm^2, n_{WT} = 137. *** *t* test $p < 0.001$. (C) Western blotting against actin on total lysates or lysates from isolated brush borders (loaded for equal total protein). (D and E) Transmission electron micrographs of isolated brush borders from (D) WT and (E) VEP$^{-/-}$ mice. Typical isolated brush borders are shown in insets (left: Nomarski; right, phalloidin staining). Arrowheads highlight actin-membrane bridges. Scale bars: 200 nm.

regular bundle pattern resembling striae (Figure 3D). The short or missing rootlets in VEP$^{-/-}$ mice look similar to those reported for P$^{-/-}$ mice (Grimm-Gunter *et al.*, 2009). Actin-membrane bridges, known to be myosin-1a–based in WT animals, could still be detected in some VEP$^{-/-}$ samples (Figure 3, D and E, arrowheads). These bridges cannot be detected in all sectioned microvilli, even in WT mice; therefore their number and arrangement cannot be reliably evaluated. Taken together, these data indicate that although actin filaments are still present in VEP$^{-/-}$ microvilli, they are sparse and no longer packed in parallel bundles.

As VEP$^{-/-}$ mice have reduced microvillar transverse area and length, their intestine absorptive surface could be significantly compromised and have an impact on growth. On the basis of the measured length, area, and density of microvilli in WT, EP$^{-/-}$, and VEP$^{-/-}$ intestine, we calculated the respective brush border membrane surfaces per square micrometer of apical domain, approximating microvilli to cylinders ($S_{WT} = 24.8 \pm 6.9\ \mu m^2$, $S_{EP-/-} = 12.0 \pm 2.5\ \mu m^2$, $S_{VEP-/-} = 14.4 \pm 2.8\ \mu m^2$; maximal SDs were calculated according to the Gaussian error-propagation law). The brush border membrane surface was strongly reduced in VEP$^{-/-}$ enterocytes compared with WT, but not EP$^{-/-}$, enterocytes. As the EP$^{-/-}$ and VEP$^{-/-}$ absorptive surfaces are similar, the effect of smaller microvilli on the VEP$^{-/-}$ growth retardation phenotype can be ruled out. The growth delay of VEP$^{-/-}$ mice is thus not due to a reduction in the absorptive surface of the epithelium but could be linked to a defect in actin bundle organization.

Digestive enzymes do not properly localize in the apical domain

One important step toward understanding the phenotype of the VEP$^{-/-}$ mice is to define how the disorganization of the actin network accounts for growth retardation. Trafficking toward the basolateral domain did not appear to be affected, as illustrated by the basolateral localization of the Na^+/K^+-ATPase in VEP$^{-/-}$ enterocytes (Figure S3B). We therefore analyzed the localization of digestive enzymes that are normally exposed at the apical surface of the enterocytes using a variety of apical trafficking routes. As the VEP$^{-/-}$ mouse demonstrates the major terminal web defects previously reported in the plastin-1 KO (Grimm-Gunter *et al.*, 2009), and as we need to unravel the specificity of the VEP$^{-/-}$ samples, we used both WT and P$^{-/-}$ samples as controls in this study (Figure 4). The lipid raft–associated aminopeptidase N (APN) still localized properly in the VEP$^{-/-}$ brush border (Figure S3A). Nevertheless, several enzymes presented an impressive subapical accumulation in the VEP$^{-/-}$ enterocytes, with partial localization in the microvilli (Figure 4A, stars). This was the case for raft-independent lactase phlorizin hydrolase (LPH), raft-associated sucrase-isomaltase (SI), and peptide transporter protein PepT1. Moreover, Western blot analyses performed on lysates from purified brush borders showed that the amount of these enzymes that still localized to the microvilli was reduced in the VEP$^{-/-}$ compared with the WT or P$^{-/-}$ samples (Figure 4B). To a much lesser extent, LPH could be seen accumulating subapically in some areas of the plastin-1 KO (Figure 4A) and its combinations (Figure S2). In the VP$^{-/-}$ enterocytes, SI also appeared delocalized and PepT1 showed some slight subapical accumulation but much less strikingly than in the VEP$^{-/-}$ samples (Figure S2). The amount of dipeptidyl-peptidase IV (DPPIV), an enzyme following a transcytotic pathway, was strongly reduced in the VEP$^{-/-}$ microvilli, as demonstrated both by Western blotting (Figure 4B) and immunostaining (Figure 4A, circle), but DPPIV did not show the intense subapical accumulations reported above. Finally, the glycosylphosphatidylinositol-anchored intestinal alkaline phosphatase (IAP) presented both a very strong decrease in the VEP$^{-/-}$ brush border, observed by Western blotting and immunostaining, and a significant subapical accumulation (Figure 4, A, star and circle, and B). The subapical accumulations reported by immunofluorescence were in agreement with the high vesicular content of the VEP$^{-/-}$ cytoplasm detected by TEM (Figure 2). Compared with the WT cell and brush border lysates, a reproducible shift in the size of the bands detected by Western blotting occurred for LPH, SI, DPPIV, and APN in the P$^{-/-}$ and VEP$^{-/-}$ samples (Figures 4A and S3A). This shift could be suppressed by treating the samples with glycosidases and therefore reflects a difference in the glycosylation pattern (Figure S5). This unexpected phenomenon is not responsible for the phenotype of the VEP$^{-/-}$ mice, because it already occurs in the P$^{-/-}$ samples and thus must be due solely to the depletion of plastin-1.

To directly assess an absorption defect in the VEP$^{-/-}$ mice, we measured the kinetics of glucose absorption of fasted WT, P$^{-/-}$, and VEP$^{-/-}$ mice following oral glucose load. The glucose absorptive capacity of VEP$^{-/-}$ intestine was strongly and significantly reduced compared with both WT and P$^{-/-}$ animals, as depicted by the measurements of glucose blood level plotted against time after gavage (Figure 4C). Interestingly, the blood glucose level in VEP$^{-/-}$ mice was significantly reduced by 75% at 30 min. Such an early time point directly represents an alteration of the glucose absorption capacity of the enterocytes, as the adaptive physiological response to high glycemia has not yet occurred.

The study of the triple KO enterocytes therefore reveals a major disruption in apical delivery and/or retention of enzymes at the apical membrane associated with malabsorption and subsequent growth delay that develops predominantly after weaning in the VEP$^{-/-}$ mice. The slight apical localization defects observed in the VP$^{-/-}$ samples are not sufficient to cause such a growth delay in these mice (Figure 1B).

Apical membrane retention is deficient and myosin-1a is mislocalized

To decipher the apical transport or anchorage mechanisms that are defective in the VEP$^{-/-}$ mice, we analyzed the subcellular localization of several players in apical targeting and delivery. The organization of the Golgi was not affected in the VEP$^{-/-}$ enterocytes, as the Golgi marker giantin and the GTP-binding protein Rab6, which is implicated in intra-Golgi transport, retained the localization observed in WT enterocytes (Figure S4A). The Golgi apparatus appeared morphologically unaltered, suggesting that a later step in the apical transport could be defective. Cargoes are known to go through Rab11- and Rab8-positive compartments en route to the apical pole. Although the subnuclear localization of Rab11 was not affected in the VEP$^{-/-}$ animals (Figure S4A), Rab8 subapical concentration looked slightly decreased when observed by immunofluorescence (Figure S4B). However, this reduced Rab8 apical localization could not be confirmed by Western blotting (Figure S4B). Whereas the apical delivery route did not appear affected, the early endosomal marker EEA1 exhibited an enlarged subapical localization in the VEP$^{-/-}$ enterocytes (Figure 5A) and strongly colocalized with the accumulation of apical markers, as shown for SI (Figure 5B). These results suggest that endocytosis, rather than apical delivery, is responsible for the mislocalization of apical enzymes and transporters in the VEP$^{-/-}$ mice. Is endocytosis therefore enhanced in the absence of a proper actin bundle or are these apical components more prone to endocytosis? To discriminate between these two possibilities, we compared in vivo the kinetics of global endocytosis using the vital membrane stain FM dye as an endocytic probe perfused in the intestinal lumens of WT and

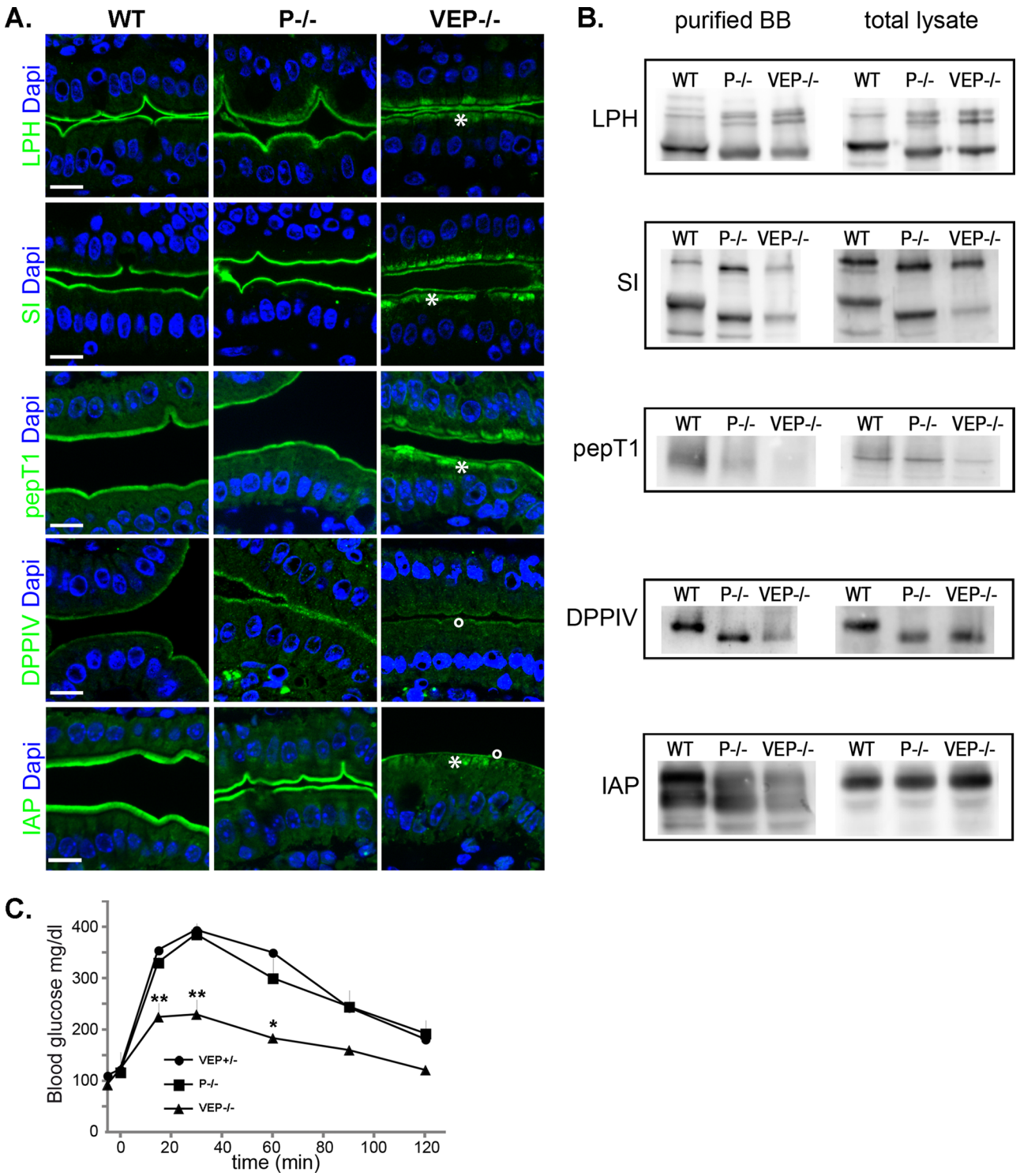

FIGURE 4: VEP$^{-/-}$ mice show apical localization defects of major digestive and absorptive brush border components. (A) Histological sections of jejunum from WT, P$^{-/-}$ and VEP$^{-/-}$ animals immunostained for LPH, SI, PepT1, DPPIV, and IAP (green). DAPI (blue) labels nuclei. Scale bars: 10 μm. (B) Western blots against LPH, SI, PepT1, DPPIV, and IAP were performed on total or isolated brush borders lysates (loaded for equal total protein). (C) Blood glucose concentrations plotted over time during oral glucose tolerance test in mice fasted overnight ($n_{VEP+/-}$ = 3; $n_{P-/-}$ = 5; $n_{VEP-/-}$ = 3; Mann-Whitney: **, $p < 0.01$, *, $p < 0.05$).

VEP$^{-/-}$ mice (Hansen *et al.*, 2009). A modification in the internalization of the dye in the KO enterocytes could not be detected at any of the time points analyzed from 5 to 90 min (Figure 5C). The global endocytosis rate is therefore not increased in the VEP$^{-/-}$ enterocytes, and the accumulation of apical digestive components in EEA1-positive compartments is most likely due to their deficient stabilization at the apical membrane.

The mechanisms allowing membrane retention of apical enzymes and transporters are widely unknown. To date, only the actin motor myosin-1a, a brush border myosin, has been implicated in the

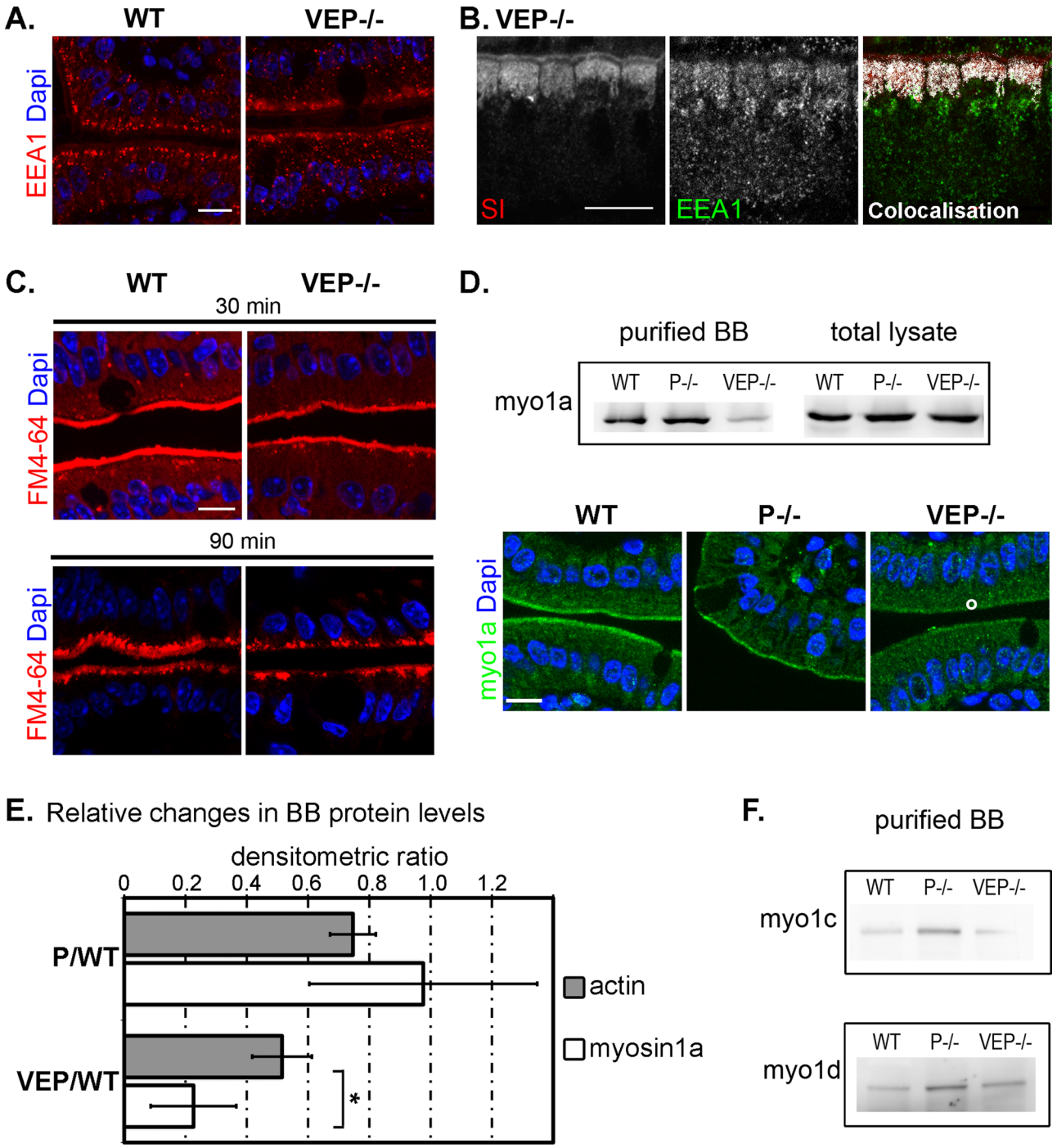

FIGURE 5: The apical domain retention machinery is affected in VEP$^{-/-}$ mice. (A) Immunostaining against the early endosomal marker EEA1 in WT and VEP$^{-/-}$ enterocytes. (B) Colocalization (white) of EEA1 (green) with the subapical accumulations of the enzyme SI (red) by immunostaining. (C) Unchanged global endocytosis rate analyzed by the internalization of the vital membrane dye FM4-64 (red), shown at 30- and 90-min time points. (D) Western blots and immunostaining against myosin-1a on WT, P$^{-/-}$, and VEP$^{-/-}$ samples. Western blot analysis was performed on total and isolated brush border lysates. DAPI labels nuclei (blue). Scale bars: 10 µm. (E) Histograms depicting the relative changes of actin and myosin-1a protein content between P$^{-/-}$ or VEP$^{-/-}$ and WT brush borders (P/WT and VEP/WT, respectively). Values are densitometric ratios of Western blotting performed on brush border lysates (P/WT: 0.98 ± 0.37, n_{myo1a} = 3, and 0.75 ± 0.07, n_{actin} = 5; VEP/WT: 0.23 ± 0.14, n_{myo1a} = 3, and 0.52 ± 0.10, n_{actin} = 5). *Wilcoxon two-sample test $p < 0.05$. (F) Western blotting performed on isolated brush border lysates against myosins-1c and -1d on WT, P$^{-/-}$, and VEP$^{-/-}$ samples showing that the decrease in myosin-1a is not accompanied by their compensatory recruitment to the brush borders.

anchorage of some apical enzymes (Tyska and Mooseker, 2004). Remarkably, whereas it is properly concentrated in the microvilli of WT and P$^{-/-}$ enterocytes, myosin-1a was substantially lost in VEP$^{-/-}$ microvilli, as detected by Western blotting on isolated brush border lysates and by immunofluorescence (Figure 5D). As the actin content was also diminished in VEP$^{-/-}$ brush borders (Figure 3C), we

wondered whether the reduction in myosin-1a was directly due to the loss of the actin-bundling proteins or solely a reflection of the lower actin content. We quantified by densitometric analysis of Western blots the relative changes in actin and myosin-1a content between WT and $P^{-/-}$ or $VEP^{-/-}$ brush borders (Figure 5E). The densitometric ratio of $P^{-/-}$ over WT brush border samples was not significantly different between actin and myosin-1a (0.98 ± 0.37, $n_{myo1a} = 3$, and 0.75 ± 0.07, $n_{actin} = 5$, $p \leq 0.8$). In contrast, the densitometric ratio of $VEP^{-/-}$ over WT brush border samples was significantly reduced for myosin-1a compared with actin (0.23 ± 0.14, $n_{myo1a} = 3$, and 0.52 ± 0.10, $n_{actin} = 5$; Mann-Whitney $p < 0.05$). This demonstrates that $VEP^{-/-}$ brush borders lost approximately two times more myosin-1a than actin and that the decrease in myosin-1a was not merely due to a decrease in brush border actin. Although myosin-1a brush border level was strongly decreased, it was not completely absent. We could still detect some myosin-1a bridges by TEM (Figure 3E), and the myosin-1a–based extrusion of vesicular membranes (McConnell and Tyska, 2007) was still detected upon ATP-induced myosin activation on isolated $VEP^{-/-}$ brush borders (Figure S6). The KO of myosin-1a in mouse enterocytes does not cause defects at the whole-animal level (Tyska *et al.*, 2005). This lack of phenotype has been accounted for by the compensatory recruitment of at least two other myosins, myosin-1c and -1d, in the brush border (Tyska *et al.*, 2005; Benesh *et al.*, 2010). We therefore used Western blotting to analyze the brush border content of these class I myosins in our samples. The level of these two myosins did not increase between $VEP^{-/-}$ and WT brush borders (Figure 5F). Neither of them became ectopically recruited to the microvilli in the absence of the three actin-bundling proteins, although myosin-1a was almost absent from $VEP^{-/-}$ microvilli. Thus the absence of the three actin-bundling proteins is associated with defects in the brush border localization of at least one player in apical enzyme retention, myosin-1a.

DISCUSSION

How to build microvilli without actin-bundling proteins?

As discussed in the *Introduction*, a number of experimental data strongly suggest a role for actin-bundling proteins in the formation of membrane protrusions. It is therefore surprising that mice devoid of actin bundlers still form microvilli. However, biophysical and modeling studies have questioned this presupposed requirement (Janmey *et al.*, 1992; Miyata *et al.*, 1999; Mogilner and Rubinstein, 2005). Actin polymerization alone would be sufficient to produce a force that can overcome the resistance of the membrane to bending (Peskin *et al.*, 1993; Mogilner and Rubinstein, 2005). Our results are in favor of such a dispensable role for actin-bundling proteins in microvilli protrusions in vivo. As actin filaments are flexible, the force they generate after reaching a critical protrusion length is limited by buckling that occurs in response to the membrane resilience force. This critical length is dependent on the number of filaments and on their rigidity, the latter being increased by their physical bundling (Mogilner and Rubinstein, 2005; Atilgan *et al.*, 2006; Claessens *et al.*, 2006; Bathe *et al.*, 2008). In agreement with these biophysical models, we demonstrate that actin-bundling proteins do not act redundantly in the protrusion of microvilli but do regulate their length. A role for plastin-1 in microvillar lengthening has already been reported in vivo (Grimm-Gunter *et al.*, 2009). In contrast to their reported roles in LLCPK-1 cells (Loomis *et al.*, 2003), we show that espin plays a positive role in regulating microvillar length only in the absence of plastin-1, whereas villin clearly has no effect. The three bundlers are therefore not equivalent in their contributions to microvillar morphogenesis. Nevertheless, they do cooperatively contribute to the paracrystalline, bundled organization of filaments that is lost in the $VEP^{-/-}$ mice compared with the single or double KO.

Although actin-bundling proteins are dispensable, many additional mechanisms can provide sufficient organization to the network for membrane protrusion to occur. It has been proposed that the membrane itself participates in the organization of actin filaments in parallel arrays within protrusions (Liu *et al.*, 2008). In stereocilia and filopodia, the role of actin-binding proteins in the tip complex is well documented (Tokuo and Ikebe, 2004; Pellegrin and Mellor, 2005; Rzadzinska *et al.*, 2009). Eps8 is localized at the tip of microvilli and participates in their morphogenesis (Croce *et al.*, 2004; Tocchetti *et al.*, 2010). Eps8 cross-linking activity (Disanza *et al.*, 2006; Hertzog *et al.*, 2010) combined with its restricted localization make it a credible molecular bond between the polymerizing ends of actin filaments. This tip connection and the remaining myosin bridges linking actin filaments to the membrane may be sufficient to maintain the longitudinal filaments observed in $VEP^{-/-}$ microvilli. Moreover, the nucleator mDia1 has been identified in our proteomic analysis. If present in the tip complex, this nucleator is likely to initiate and elongate unipolar arrays of actin filaments (Campellone and Welch, 2010), as formins do in filopodia (Mellor, 2010). In future studies, it will be of interest to investigate the function of mDia1 in microvilli.

Defective apical retention and increased internalization of membrane proteins?

The malabsorption and growth retardation reported for the $VEP^{-/-}$ mice cannot be explained by microvillar shortening, because similar shortening and reduction of membrane surface are also present in non-growth-retarded $EP^{-/-}$ mice. It is more likely due to defective enterocyte absorption caused by the large defects in the apical localization of transporters and enzymes required for this process. We demonstrate that, although the endocytic rate is unmodified, these membrane proteins accumulate in EEA1-positive compartments. SI and LPH-associated vesicles traverse endosomal compartments en route to the apical pole, but they do not normally associate with EEA1 (Cramm-Behrens *et al.*, 2008). Moreover, digestive enzymes are highly stable at the apex, presenting a very low basal rate of endocytosis and recycling (Matter *et al.*, 1990; Hansen *et al.*, 2009). Our results clearly argue in favor of a highly increased susceptibility to internalization via normal endocytic pathways in the $VEP^{-/-}$ animals. Interaction with the cytoskeleton is essential for membrane protein stabilization, but little is known about the molecular mechanisms involved (Nelson and Veshnock, 1987; Tyska and Mooseker, 2004). In enterocytes, myosin-1a has been implicated in the retention of SI within the brush border (Tyska and Mooseker, 2004; Tyska *et al.*, 2005). Its strong mislocalization in this study, in the absence of a structured actin network, provides good evidence of the general mechanism at the origin of the retention defects, but myosin-1a is most probably not the only cytoskeletal linker affected—the others being still undiscovered.

In myosin-1a KO microvilli, enzymes appear to localize fairly normally, and no overt phenotype was detected (Tyska and Mooseker, 2004; Tyska *et al.*, 2005), most probably due to compensatory recruitment of myosin-1c and -1d (Tyska *et al.*, 2005; Benesh *et al.*, 2010). This recruitment solely in the absence of myosin-1a is due to differential actin-binding affinities and competition for actin-binding sites (Tyska *et al.*, 2005; Benesh *et al.*, 2010). Equivalent ectopic redistributions are not detected in the $VEP^{-/-}$ enterocytes, even if myosin-1a is substantially lost from the microvilli. This suggests that the abnormality that affects the recruitment of myosin-1a could be

structural, residing in the disorganization of the actin network, and would hence also perturb the recruitment of any other possible compensatory class I myosin, causing the apical defects observed.

Actin bundle architecture is critical for the efficient recruitment of proteins

Compared with single and double KO microvilli, those of VEP$^{-/-}$ demonstrate an additional structural defect: the lack of organization of actin filaments into a bundle. The literature increasingly reports the importance of specific actin architecture for the selective binding of proteins (Temm-Grove *et al.*, 1998; Tang and Ostap, 2001; DesMarais *et al.*, 2002; Nagy *et al.*, 2008; Nagy and Rock, 2010; Brawley and Rock, 2009). In the VEP$^{-/-}$ enterocytes, because myosin-1 is not efficiently recruited to the microvilli, myosins are of particular interest. Different classes of unconventional myosins have been shown to select specific actin filament subpopulations in cells (Brawley and Rock, 2009). The filopodium myosin-X selects actin bundles for processive movement (Nagy *et al.*, 2008; Nagy and Rock, 2010; Ricca and Rock, 2010). Moreover, the architecture and dynamics of the bundle regulate the differential concentration of actin-binding molecules in the bundle (Naoz *et al.*, 2008). Loss of the stabilizing effect of actin-bundling proteins (Zigmond *et al.*, 1992; Tilney *et al.*, 2003; Prost *et al.*, 2007) is therefore likely to modify the localization of myosins and other associated molecules (Naoz *et al.*, 2008). Finally, the radial "barber pole" distribution of myosin-1a along the microvillar axis relies on the precise paracrystalline hexagonal arrangement of actin filaments together with the sterical hindrance generated by the bundlers (Brown and McKnight, 2010). Alterations to the concentration and localization of myosin-1a in the brush borders of VEP$^{-/-}$ mice most likely reflect the different architectural organization of the actin network. It is thus conceivable that myosin-1a, and other actin-binding proteins present in the brush border, do not efficiently bind or move along the unstructured VEP$^{-/-}$ actin network.

In conclusion, the function of actin-bundling proteins is not to power the morphogenesis of microvilli per se but to grant the actin network a precise architecture that allows the selective recruitment of proteins implicated in apical retention. This work highlights in vivo the importance of local cytoskeletal organization in the proper regulation of subcellular membrane specializations.

MATERIALS AND METHODS

KO mice

The double and triple KO mice used in this study were generated by successive crossing between the villin (Ferrary *et al.*, 1999), espin (Zheng *et al.*, 2000), and plastin-1 (Grimm-Gunter *et al.*, 2009) KO, as described previously. The espin KO (jerker) mice, which carry a natural autosomal recessive mutation in the gene encoding the bundlers of the espin family, were purchased from the Jackson Laboratory (Bar Harbor, ME). They were all genotyped by PCR. Animal experiments were carried out under the authority of the Curie Institute veterinarian, under permission granted to the Robine laboratory (number 75-433, Préfecture de Police—Direction des Services Vétérinaires de Paris).

Growth curves

To analyze the growth of VEP$^{-/-}$ animals, mice born from crosses of VEP$^{-/-}$ males with VEP$^{-/-}$ females were compared with half-siblings born from the same males crossed with WT females. The double KO VP$^{-/-}$ litters were from intercrosses of double KO parents. The weights of 86 mice from 12 different litters with the three different genotypes were measured every 2 d during the first 60 d after birth. We analyzed the growth time series by adjusting a mixed-effect model in order to assess the significance of the genotype effect. The fixed effects accounted for in the model are the genotype, the sex, and the time, while the litter is considered a random effect. For more details, see Supplemental Material.

Sampling and preparation of the tissues

The intestine of adult mice was isolated and divided into three parts of identical length corresponding to the duodenum, jejunum, and ileum. The intestinal tube was washed with phosphate-buffered saline (PBS). To prepare tissue for paraffin sectioning, we fixed short pieces of jejunum in 4% paraformaldehyde (PFA), in Carnoy solution (60% ethanol, 30% chloroform, 10% acetic acid), or in 70% methanol for 2 h at room temperature or overnight at 4°C. The samples were then ethanol- or methanol-dehydrated and embedded in paraffin. For cryosections, tissues were fixed for 2 h in PFA and incubated overnight in a 30% glucose solution. They were then embedded in optimal cutting temperature compound (OCT) and frozen at −80°C. For histological analysis, sections of 5 µm were prepared from paraffin-embedded tissues and stained with hematoxylin eosin–safranin according to standard histological procedures.

Oral glucose tolerance test

Mice were fasted overnight and then received a glucose load of 4 mg/kg. The blood glucose level was assessed at different time points using an ACCU-CHEK Compact Plus meter system (Roche, Basel, Switzerland). At least three animals per genotype were included in the study.

Immunohistochemistry

Sections of 5 µm were prepared from paraffin- or OCT-embedded tissues depending on the antibody used. For paraffin sections, paraffin was removed by two 5-min washes in xylene. Sections were then hydrated with ethanol solutions of decreasing concentrations. Unmasking of the epitopes was performed by boiling for 20 min in Antigen Unmasking Solution (Vector Laboratories, Burlingame, CA). Sections were incubated for 45 min at room temperature in blocking buffer (3% fetal calf serum [FCS] in PBS) and then overnight at 4°C with primary antibody (see Supplemental Material) diluted in 3% FCS. After several washes, secondary fluorescent antibody was added for 90 min. Representative images from immunostaining were acquired using an Apotome system with a 63× water Plan-Apochromat lens (Zeiss, Jena, Germany). All images were further processed and pseudocolored using ImageJ (National Institutes of Health). All images comparing different genotypes were acquired and postprocessed with identical parameters. Colocalization analyses were performed using the Colocalization Highlighter plug-in for ImageJ.

TEM

Small pieces of tissue (~1–2 mm) were fixed for 2 h at room temperature in 2.5% glutaraldehyde and 2% PFA in cacodylate buffer (80 mM cacodylate buffer, pH 7.2, 0.05% $CaCl_2$). After being washed with cacodylate buffer, tissues were postfixed for 30 min at 4°C with 1% OsO_4 and 1.5% potassium ferrocyanide in 80. mM cacodylate buffer (pH 7.2), and then treated at room temperature for 1 h with 2% uranyl acetate in 40% ethanol. The samples were dehydrated in a series of graded ethanol solutions and then embedded in Epon before ultrathin sectioning. The observations were made with a Philips CM120 electron microscope (FEI, Eindhoven, The Netherlands). Images were acquired with a KeenView camera,

and measurements were made with the iTEM software (Olympus Soft Imaging Solutions GMBH, Münster, Germany).

Brush border isolation

Intestines from two adult mice were collected, cut into three pieces, and soaked in ice cold saline (150 mM NaCl, 2 mM imidazole, pH 7.2). Segments were washed with saline and opened longitudinally. They were then cut into pieces (~2 cm) and stirred in a beaker containing 20 ml of ice cold sucrose dissociation solution buffer A (200 mM sucrose, 12 mM EDTA, 19 mM KH_2PO_4, 78 mM Na_2HPO_4) for 30 min in a cold room. The buffer A containing the enterocytes was centrifuged at 300 × *g* for 8 min. During this spin, another 20 ml of buffer A was poured into the beaker and stirred. This second 20-ml cell collection was added to the cell pellets obtained from the first collection. The isolated enterocytes were washed three times in buffer A by centrifugation at 300 × *g* for 8 min. The cell pellet was then resuspended with 20 ml of homogenization buffer (10 mM imidazole, pH 7.2, 4 mM EDTA, 1 mM ethylene glycol tetraacetic acid [EGTA], 1 mM dithiothreitol [DTT], protease inhibitor cocktail [Sigma-Aldrich, St. Louis, MO], pH 7.2), poured into a blender, and homogenized with two 15-s bursts at high speed. The blender was rinsed once with 20 ml of buffer B (75 mM KCl, 5 mM $MgCl_2$, 1 mM EGTA, 10 mM imidazole, pH 7.4, 1 mM DTT, and protease inhibitor cocktail). The homogenate was then centrifuged (1000 × *g* for 8 min) to pellet the brush borders. The pellet containing isolated brush borders was washed four times by centrifugation in buffer B (1000 × *g* for 8 min).

For TEM, isolated brush borders were incubated in buffer B containing 15 mM $MgCl_2$. To let them adhere, they were incubated for 1 h at 4°C on glass coverslips coated with polylysine. Coverslips were washed once before fixation in 0.1 M Na-phosphate buffer (pH 7.0) containing 2% glutaraldehyde and 2 mg/ml tannic acid for 1 h at 4°C. After being washed in PBS, brush borders were postfixed in 1% OsO_4, in 0.1 M phosphate buffer at pH 6.0 for 45 min and then with 0.5% uranyl acetate for 2 h. The brush borders were dehydrated in a series of graded ethanol solutions and then embedded in Epon before ultrathin sectioning.

For one-dimensional analysis, brush border pellets were frozen in liquid nitrogen and kept at −80°C before being processed as described in the following section. For Western blotting, the pellets were processed the same way as for tissue samples.

Tissue lysis and Western blotting

Frozen jejunal tissues were homogenized with a Dounce homogenizer in a solution containing 50 mM Tris- HCl (pH 7.5), 150 mM NaCl, 20 mM MgCl2, 5 mM EDTA, 1% Triton X-100, 1% NP-40, 0.5% SDS, and protease inhibitor cocktail (Sigma-Aldrich, St. Louis, MO). Proteins were extracted after centrifugation at 15,000 × *g* for 10 min at 4°C. Fifty micrograms of total protein was used for electrophoresis on 7.5% SDS-polyacrylamide gels under reducing conditions, and transferred to a nitrocellulose membrane using standard procedures. Immunogens were visualized using the enhanced chemiluminescence method (Thermo Scientific, Lafayette, CO). The primary antibodies used for immunoblots in these experiments were the same as those described for immunohistochemistry, and were used at 1:1000. In addition, polyclonal rabbit β-actin (Cell Signaling Technology, Danvers, MA), monoclonal mDia1 (BD Biosciences, Franklin Lakes, NJ), polyclonal rabbit myosin-1c (from P. Gillespie), polyclonal rabbit anti–myosin-1d (from M. Bähler), and monoclonal IRSp53 (from G. Scita) antibodies were used, also at 1:1000. Harmonin isoforms were detected using a rabbit serum at 1:200 (from C. Petit). Protein lysates were deglycosylated using the Protein Deglycosylation Mix (New England BioLabs, Ipswich, MA).

Densitometry measurements were carried out using the software ImageJ. The densitometric value of each band was corrected by subtracting the background value of the corresponding lane before applying the ratio calculations.

Global endocytosis assay

Intestinal segments from anesthetized mice were isolated using sewing cotton. A solution of the vital membrane stain FM4-64 FX (Invitrogen, Carlsbad, CA) diluted in PBS-$MgCl_2$-$CaCl_2$ at 100 µg/ml was injected into the isolated segments and incubated for different times at 37°C. The mice were then killed, and isolated segments were fixed and processed for cryosectioning. Endocytic activity was assessed by the internalization of labeled membranes observed by fluorescence microscopy.

ACKNOWLEDGMENTS

We are grateful to A. Quaroni (Cornell University), R. Jacob (Philipps-Universität Marburg, Marburg, Germany), E.M. Danielsen (Panum Institute, University of Copenhagen, Denmark), A.L. Hubbard (Johns Hopkins University, Baltimore, MD), G. Kellett (University of York, Heslington, UK), F. Jaisser (INSERM U872, Centre de recherche des Cordeliers, Paris, France), M. Mooseker (Yale University, New Haven, CT), P.G. Gillepsie (Oregon Health & Science University, Portland, OR), M. Bähler (Westfälische Wilhems-Universität Münster, Münster, Germany), J. Klingensmith (Duke University, Durham, NC), C. Petit (Institut Pasteur, Paris, France), and T. Galli (Institut Jacques Monod, Paris, France) for kindly supplying antibodies. We thank G. Raposo for the collaboration on TEM and M. Arpin, E. Coudrier, E. Ferrary, D. Vignjevic, and S. Duffy for advice and careful reading of the manuscript. We thank J. Mandel and the bioinformatics platform for the analysis of the growth curves; all members of the animal house facility and in particular Stéphanie Boissel; C. Backeland, W. Faigle, and V. Masson from the proteomics platform; and the PICT@BDD imaging facility, especially O. Renaud and O. Leroy. The Curie Institute Foundation funded this work. C.R. was supported by the CNRS and Association pour la Recherche sur le Cancer; F.U. was supported by the Ministère de la Recherche et de la Technologie and by Fondation pour la Recherche Médicale. The Laboratory of Proteomic Mass Spectrometry is supported by Cancéropôle Ile-de-France and Institut National du Cancer (INCA).

REFERENCES

Atilgan E, Wirtz D, Sun SX (2006). Mechanics and dynamics of actin-driven thin membrane protrusions. Biophys J 90, 65–76.

Bartles JR (2000). Parallel actin bundles and their multiple actin-bundling proteins. Curr Opin Cell Biol 12, 72–78.

Bathe M, Heussinger C, Claessens MM, Bausch AR, Frey E (2008). Cytoskeletal bundle mechanics. Biophys J 94, 2955–2964.

Benesh AE, Nambiar R, McConnell RE, Mao S, Tabb DL, Tyska MJ (2010). Differential localization and dynamics of class I myosins in the enterocyte microvillus. Mol Biol Cell 21, 970–978.

Boeda B *et al.* (2002). Myosin VIIa, harmonin and cadherin 23, three Usher I gene products that cooperate to shape the sensory hair cell bundle. EMBO J 21, 6689–6699.

Brawley CM, Rock RS (2009). Unconventional myosin traffic in cells reveals a selective actin cytoskeleton. Proc Natl Acad Sci USA 106, 9685–9690.

Brown JW, McKnight CJ (2010). Molecular model of the microvillar cytoskeleton and organization of the brush border. PLoS One 5, e9406.

Campellone KG, Welch MD (2010). A nucleator arms race: cellular control of actin assembly. Nat Rev Mol Cell Biol 11, 237–251.

Claessens MM, Bathe M, Frey E, Bausch AR (2006). Actin-binding proteins sensitively mediate F-actin bundle stiffness. Nat Mater 5, 748–753.

Coluccio LM, Bretscher A (1989). Reassociation of microvillar core proteins: making a microvillar core in vitro. J Cell Biol 108, 495–502.

Costa de Beauregard MA, Pringault E, Robine S, Louvard D (1995). Suppression of villin expression by antisense RNA impairs brush border assembly in polarized epithelial intestinal cells. EMBO J 14, 409–421.
Cramm-Behrens CI, Dienst M, Jacob R (2008). Apical cargo traverses endosomal compartments on the passage to the cell surface. Traffic 9, 2206–2220.
Croce A, Cassata G, Disanza A, Gagliani MC, Tacchetti C, Malabarba MG, Carlier MF, Scita G, Baumeister R, Di Fiore PP (2004). A novel actin barbed-end-capping activity in EPS-8 regulates apical morphogenesis in intestinal cells of *Caenorhabditis elegans*. Nat Cell Biol 6, 1173–1179.
DesMarais V, Ichetovkin I, Condeelis J, Hitchcock-DeGregori SE (2002). Spatial regulation of actin dynamics: a tropomyosin-free, actin-rich compartment at the leading edge. J Cell Sci 115, 4649–4660.
Disanza A *et al*. (2006). Regulation of cell shape by Cdc42 is mediated by the synergic actin-bundling activity of the Eps8-IRSp53 complex. Nat Cell Biol 8, 1337–1347.
Ferrary E *et al*. (1999). In vivo, villin is required for Ca^{2+}-dependent F-actin disruption in intestinal brush borders. J Cell Biol 146, 819–830.
Franck Z, Footer M, Bretscher A (1990). Microinjection of villin into cultured cells induces rapid and long-lasting changes in cell morphology but does not inhibit cytokinesis, cell motility, or membrane ruffling. J Cell Biol 111, 2475–2485.
Friederich E, Huet C, Arpin M, Louvard D (1989). Villin induces microvilli growth and actin redistribution in transfected fibroblasts. Cell 59, 461–475.
Grimm-Gunter EM, Revenu C, Ramos S, Hurbain I, Smyth N, Ferrary E, Louvard D, Robine S, Rivero F (2009). Plastin 1 binds to keratin and is required for terminal web assembly in the intestinal epithelium. Mol Biol Cell 20, 2549–2562.
Gruneberg H, Burnett JB, Snell GD (1941). The origin of jerker, a new gene mutation of the house mouse, and linkage studies made with it. Proc Natl Acad Sci USA 27, 562–565.
Hansen GH, Rasmussen K, Niels-Christiansen LL, Danielsen EM (2009). Endocytic trafficking from the small intestinal brush border probed with FM dye. Am J Physiol Gastrointest Liver Physiol 297, G708–G715.
Hertzog M *et al*. (2010). Molecular basis for the dual function of Eps8 on actin dynamics: bundling and capping. PLoS Biol 8, e1000387.
Hirokawa N, Cheney RE, Willard M (1983). Location of a protein of the fodrin-spectrin-TW260/240 family in the mouse intestinal brush border. Cell 32, 953–965.
Hirokawa N, Tilney LG, Fujiwara K, Heuser JE (1982). Organization of actin, myosin, and intermediate filaments in the brush border of intestinal epithelial cells. J Cell Biol 94, 425–443.
Janmey PA, Lamb J, Allen PG, Matsudaira PT (1992). Phosphoinositide-binding peptides derived from the sequences of gelsolin and villin. J Biol Chem 267, 11818–11823.
Liu AP, Richmond DL, Maibaum L, Pronk S, Geissler PL, Fletcher DA (2008). Membrane-induced bundling of actin filaments. Nat Phys 4, 789–793.
Loomis PA, Zheng L, Sekerkova G, Changyaleket B, Mugnaini E, Bartles JR (2003). Espin cross-links cause the elongation of microvillus-type parallel actin bundles in vivo. J Cell Biol 163, 1045–1055.
Matter K, Stieger B, Klumperman J, Ginsel L, Hauri HP (1990). Endocytosis, recycling, and lysosomal delivery of brush border hydrolases in cultured human intestinal epithelial cells (Caco-2). J Biol Chem 265, 3503–3512.
McConnell RE, Tyska MJ (2007). Myosin-1a powers the sliding of apical membrane along microvillar actin bundles. J Cell Biol 177, 671–681.
Mellor H (2010). The role of formins in filopodia formation. Biochim Biophys Acta 1803, 191–200.
Miyata H, Nishiyama S, Akashi K, Kinosita K., Jr. (1999). Protrusive growth from giant liposomes driven by actin polymerization. Proc Natl Acad Sci USA 96, 2048–2053.
Mogilner A, Rubinstein B (2005). The physics of filopodial protrusion. Biophys J 89, 782–795.
Nagy S, Ricca BL, Norstrom MF, Courson DS, Brawley CM, Smithback PA, Rock RS (2008). A myosin motor that selects bundled actin for motility. Proc Natl Acad Sci USA 105, 9616–9620.
Nagy S, Rock RS (2010). Structured post-IQ domain governs selectivity of myosin X for fascin-actin bundles. J Biol Chem 285, 26608–26617.
Naoz M, Manor U, Sakaguchi H, Kachar B, Gov NS (2008). Protein localization by actin treadmilling and molecular motors regulates stereocilia shape and treadmilling rate. Biophys J 95, 5706–5718.
Nelson WJ, Veshnock PJ (1987). Ankyrin binding to (Na^+ + K^+)ATPase and implications for the organization of membrane domains in polarized cells. Nature 328, 533–536.
Pellegrin S, Mellor H (2005). The Rho family GTPase Rif induces filopodia through mDia2. Curr Biol 15, 129–133.
Peskin CS, Odell GM, Oster GF (1993). Cellular motions and thermal fluctuations: the Brownian ratchet. Biophys J 65, 316–324.
Pinson KI, Dunbar L, Samuelson L, Gumucio DL (1998). Targeted disruption of the mouse villin gene does not impair the morphogenesis of microvilli. Dev Dyn 211, 109–121.
Prost J, Barbetta C, Joanny JF (2007). Dynamical control of the shape and size of stereocilia and microvilli. Biophys J 93, 1124–1133.
Revenu C, Athman R, Robine S, Louvard D (2004). The co-workers of actin filaments: from cell structures to signals. Nat Rev Mol Cell Biol 5, 635–646.
Ricca BL, Rock RS (2010). The stepping pattern of myosin X is adapted for processive motility on bundled actin. Biophys J 99, 1818–1826.
Rodriguez-Boulan E, Kreitzer G, Musch A (2005). Organization of vesicular trafficking in epithelia. Nat Rev Mol Cell Biol 6, 233–247.
Rzadzinska AK, Nevalainen EM, Prosser HM, Lappalainen P, Steel KP (2009). MyosinVIIa interacts with Twinfilin-2 at the tips of mechanosensory stereocilia in the inner ear. PLoS One 4, e7097.
Saotome I, Curto M, McClatchey AI (2004). Ezrin is essential for epithelial organization and villus morphogenesis in the developing intestine. Dev Cell 6, 855–864.
Sato T *et al*. (2007). The Rab8 GTPase regulates apical protein localization in intestinal cells. Nature 448, 366–369.
Tang N, Ostap EM (2001). Motor domain-dependent localization of myo1b (myr-1). Curr Biol 11, 1131–1135.
Temm-Grove CJ, Jockusch BM, Weinberger RP, Schevzov G, Helfman DM (1998). Distinct localizations of tropomyosin isoforms in LLC-PK1 epithelial cells suggests specialized function at cell–cell adhesions. Cell Motil Cytoskeleton 40, 393–407.
Tilney LG, Connelly PS, Ruggiero L, Vranich KA, Guild GM (2003). Actin filament turnover regulated by cross-linking accounts for the size, shape, location, and number of actin bundles in *Drosophila* bristles. Mol Biol Cell 14, 3953–3966.
Tilney LG, Connelly PS, Vranich KA, Shaw MK, Guild GM (1998). Why are two different cross-linkers necessary for actin bundle formation in vivo and what does each cross-link contribute? J Cell Biol 143, 121–133.
Tilney LG, Tilney MS (1988). The actin filament content of hair cells of the bird cochlea is nearly constant even though the length, width, and number of stereocilia vary depending on the hair cell location. J Cell Biol 107, 2563–2574.
Tilney LG, Tilney MS, Guild GM (1995). F actin bundles in *Drosophila* bristles. I. Two filament cross-links are involved in bundling. J Cell Biol 130, 629–638.
Tocchetti A *et al*. (2010). Loss of the actin remodeler Eps8 causes intestinal defects and improved metabolic status in mice. PLoS One 5, e9468.
Tokuo H, Ikebe M (2004). Myosin X transports Mena/VASP to the tip of filopodia. Biochem Biophys Res Commun 319, 214–220.
Tyska MJ, Mackey AT, Huang JD, Copeland NG, Jenkins NA, Mooseker MS (2005). Myosin-1a is critical for normal brush border structure and composition. Mol Biol Cell 16, 2443–2457.
Tyska MJ, Mooseker MS (2004). A role for myosin-1A in the localization of a brush border disaccharidase. J Cell Biol 165, 395–405.
Verpy E *et al*. (2000). A defect in harmonin, a PDZ domain-containing protein expressed in the inner ear sensory hair cells, underlies Usher syndrome type 1C. Nat Genet 26, 51–55.
Vignjevic D, Kojima S, Aratyn Y, Danciu O, Svitkina T, Borisy GG (2006). Role of fascin in filopodial protrusion. J Cell Biol 174, 863–875.
Weisz OA, Rodriguez-Boulan E (2009). Apical trafficking in epithelial cells: signals, clusters and motors. J Cell Sci 122, 4253–4266.
Yamashiro S, Yamakita Y, Ono S, Matsumura F (1998). Fascin, an actin-bundling protein, induces membrane protrusions and increases cell motility of epithelial cells. Mol Biol Cell 9, 993–1006.
Zheng L, Sekerkova G, Vranich K, Tilney LG, Mugnaini E, Bartles JR (2000). The deaf jerker mouse has a mutation in the gene encoding the espin actin-bundling proteins of hair cell stereocilia and lacks espins. Cell 102, 377–385.
Zigmond SH, Furukawa R, Fechheimer M (1992). Inhibition of actin filament depolymerization by the *Dictyostelium* 30,000-D actin-bundling protein. J Cell Biol 119, 559–567.